2D AND 3D COLLIMATOR IMPEDANCE MODELING AND EXPERIMENTAL MEASUREMENTS

N. Biancacci, D. Amorim, S. Antipov, G. Mazzacano, B. Salvant, E. Métral,
CERN, Geneva, Switzerland
O. Frasciello, M. Zobov, INFN-LNF, Frascati, Italy
A. Mostacci, University of Rome "La Sapienza", Rome, Italy

Abstract

In order to safely operate high energy particle accelerators, an advanced collimation system in terms of absorber material choice, alignment precision and low impedance impact is often required.

In this work we will summarize the recent advancement on collimator impedance modeling starting from simple 2D structures, involving resistive jaws and transition tapers, to complex 3D structures, involving multilayer coatings, embedded beam position monitors, contact fingers, and jaw segmentation.

Measurements techniques based on the stretched and resonant wire methods will be presented in order to support simulations, together with DC and RF resistivity measurements of the jaw material samples. Recent single collimator beam based measurements will be presented as well.

INTRODUCTION

Collimators are one of the most critical equipment in high energy particle accelerators: among several requirements [1], they are used to protect the sensitive machine elements from unavoidable regular and irregular beam losses (e.g. unforeseen beam loss on the superconducting magnets in the LHC); to remove high amplitude/momentum particles; to reduce beam-induced backgrounds in the experimental areas.

Modern collimators, as the one shown in Fig. 1, are constituted by two absorbing jaws of composite materials, RF fingers to ensure good electrical contact for any jaw gap aperture, tapered sections before the main jaws for beam coupling impedance reduction, embedded BPM buttons for fast alignment relative to the beam.

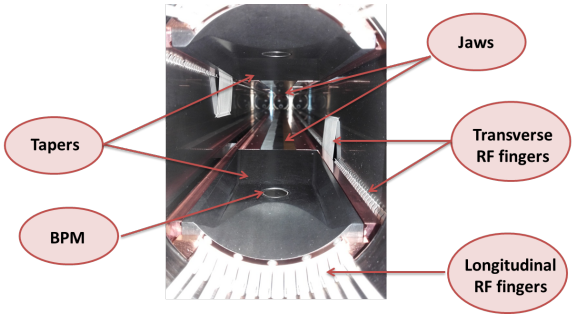

Figure 1: Example of a vertical collimator used for low impedance tests in the LHC: RF fingers, tapered transitions with embedded BPM buttons and main jaws are highlighted.

In the LHC, the collimation system is conceived in order to protect the machine from the 360 MJ circulating beams [1–3]. Two main cleaning points are present: IR3 for momentum and IR7 for betatron cleaning. Collimators are sequenced in a staged approach: primaries (TCP) intercept particles in the primary beam halo, secondaries (TCS) intercept particle scattered from the TCPs, shower absorbers (TCL) clean out remaining leakages from the previous stages. Together with these, additional collimators are installed to protect the machine against injection (TDI) and extraction (TCDQ) failures, and to protect the experiments (TCT) from remnant not cleaned particles.

Due to the proximity to the beam, the material resistivity and to the number of collimators, the LHC collimation system represents one of the major contributions to the total machine impedance budget [4] and contribute to a large fraction of the total octupole strength necessary to stabilize the beam against impedance related instabilites [5].

Due to the large impact on the LHC impedance budget, a careful estimation of the collimator impedance is mandatory in order to correctly predict the limits of stability in the context of the future HL-LHC project [6] when the beam intensity will be doubled with respect to the present LHC operational scenario [7]. This is also essential in order to quantify the possible gain in impedance reduction using different jaw materials or tapering geometry.

In the frame of impedance simulations, two approaches can be followed: a 2D or a 3D approach. In the following sections we will describe the approximations behind the two approaches together with comparisons with bench and beam measurements.

2D COLLIMATOR IMPEDANCE MODELING

A collimator can be approximated as a sequence of a tapered section, the main jaw and again a tapered section. This approach, of course, neglects any coupling between the elements, the possibility to develop resonant modes in the whole structure or the effect of the finite width and length of the collimator jaw. Nevertheless it has been proven to be sufficient for reproducing the impedance of the single device [8, 9] in dedicated LHC machine development sessions, and for quickly building the full LHC collimator impedance model for different settings scenarios. Moreover, it can be used to validate benchmark studies with 3D numerical solvers.

2519-8084 –
https://doi.org/10.23732/CYRCP-2018-001.17

Taper impedance

The impedance of taper structures with arbitrary cross section was calculated by G.Stupakov in [10]. The dipolar impedance for a vertical taper with rectangular cross section is given by

$$Z_y^{dip} = \frac{jwZ_0}{4}\int_{-\infty}^{+\infty}\frac{(g')^2}{g^3}\,\mathrm{d}z, \qquad (1)$$

with w the width in the horizontal direction, $g = g(z)$ the gap of the taper in the vertical direction, $Z_0 = 120\pi$ the characteristic impedance of vacuum. The expression in Eq. (1) is valid for $g \ll w \ll l$ with l length of the tapered transition, and for relatively low frequencies. An extensive work of benchmark and optimization of the taper geometry for the LHC collimators was done in [11, 12]. Figure 2 shows the comparison of GdfidL [13] simulations against the formula of Eq. (1) for a flat tapered collimator transition: the agreement is very good. For reference, the simulations are also compared with the impedance computed with Yokoya's [14] model for a taper with circular cross-section as used in the early LHC impedance model: the impedance is seen to be drastically underestimated with respect to the flat taper model.

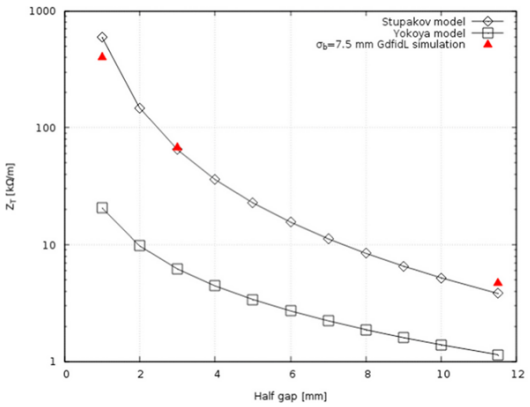

Figure 2: Effective vertical dipolar impedance for a flat tapered collimator transition: comparison of GdfidL simulations against Stupakov's and Yokoya's (round taper) models.

The impact on the overall impedance of the LHC collimators is shown in Fig. 3: below 10 mm half gap, the geometrical impedance starts contributing significantly with respect to the resistive wall impedance of the LHC secondary collimators whose jaw is made of Carbon Fiber Reinforced Carbon (CFC) composite. The contribution is also significant with respect to the tungsten (W) resistive wall impedance of the TCTs starting from 4 mm half gap.

Jaw resistive wall impedance

The jaw transverse resistive wall impedance is proportional to $\sqrt{\rho}/g^3$ with ρ the jaw resistivity [15] and it can be computed in detail considering a two parallel plates geometry with the IW2D code [16]: the code is based on field matching techniques and allows impedance calculation for an arbitrary number of layers with different material properties. The validity of the model has been checked against

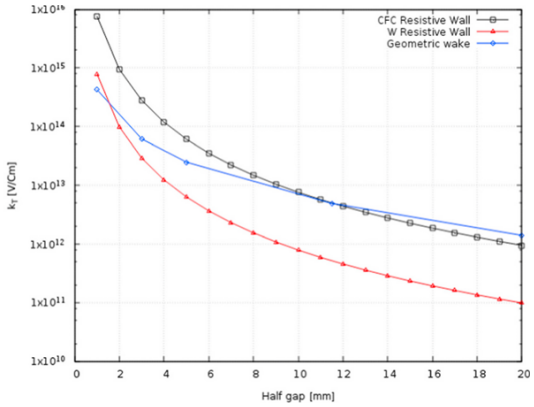

Figure 3: Impact of the geometrical impedance of the LHC taper transitions with respect to the jaw resistive wall impedance.

CST [17] simulations for the TCSPM collimator of Fig. 1. The TCSPM is a test collimator which hosts three different materials on the main jaws as shown in Fig. 4: Molybdenum (Mo), Molybdenum-graphite (MoGr) and Titanium nitride (TiN).

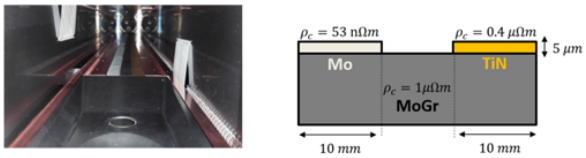

Figure 4: TCSPM jaw materials: three 10 mm wide stripes of Molybdenum (Mo), Molybdenum-graphite (MoGr) and Titanium Nitride (TiN) are present. Mo and TiN stripes are deposited with coating techniques to achieve 5 μm thickness.

Figure 5 shows the impedance computed with CST once the beam is simulated on top of each of the stripes together with comparisons with the IW2D code computation. The agreement is very good demonstrating the validity of a 2D approximation especially for low gaps. One limitation of a two parallel plates flat model is that it does not account for the width of the stripes. Figure 6 shows the impedance variation versus beam position at 1 GHz: the impedance agrees with the value corresponding to the center of the stripes within a ± 2 mm displacement which is well within the operationally achievable orbit precision.

Resonant wire impedance measurements

Bench impedance measurements were performed on the TCSPM collimator to verify its compatibility with respect to the LHC impedance requirements. As an additional value, longitudinal resonant wire impedance measurements [18] were performed in order to probe the expected impedance reduction from each of the different stripes: the wire has been horizontally shifted on top of each stripe and the corresponding impedance computed. The resonant wire method was chosen in place of the classic matched wire one thanks

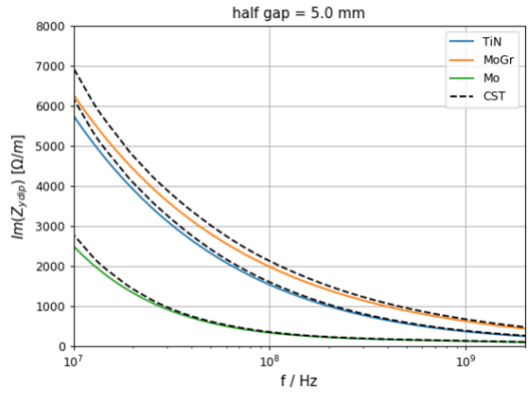

Figure 5: TCSPM resistive wall impedance computed with CST and the IW2D code. Each CST simulation curve corresponds to the beam position on the middle of the corresponding stripe.

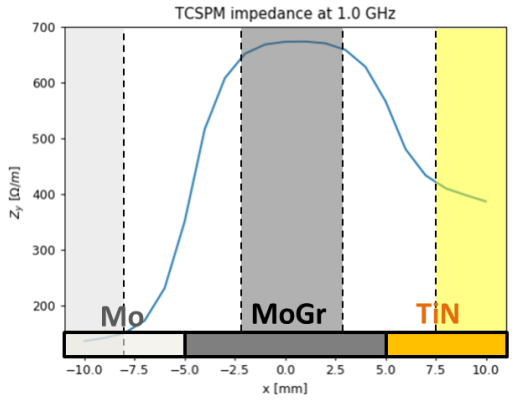

Figure 6: Resistive wall impedance versus horizontal position on the TCSPM collimator.

to the enhanced accuracy and perfect match at the resonant frequencies (see Fig. 7 for a schematic representation). We point out that the method, as applied in the TCSPM measurements, only allows the deduction of the real part of the impedance, as this is related to the change in the Q factor of the self-resonances in the DUT.

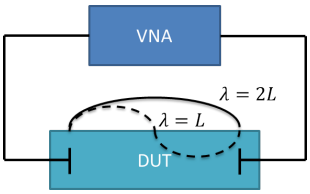

Figure 7: Resonant wire method setup: capacitors are placed at the matching sections before/after the DUT in order to produce DUT resonances at multiples of its half length.

Figure 8 shows the measured longitudinal impedance versus gap and frequency: the sampling due to the discrete number of resonances is visible as well as the presence of few higher order modes (HOMs). If, on the one hand the impedance cannot be correctly evaluated if HOMs are present due to the discrete sampling intrinsic to the method, on the other the broadband impedance can be accurately determined outside of the resonances.

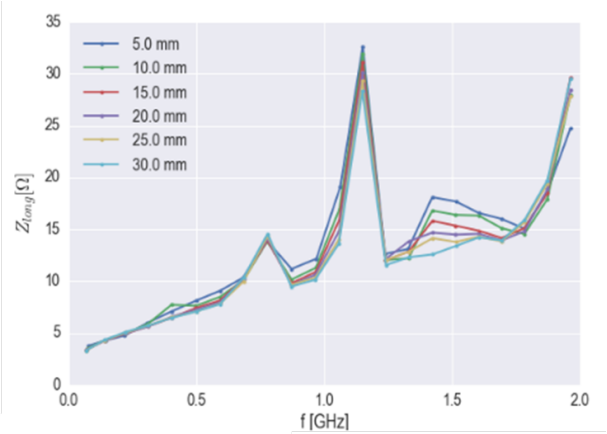

Figure 8: Longitudinal impedance versus half gap reconstructed from S21 parameters measured with the resonant wire technique. The sampling is determined by the device length.

Figure 9 shows the dependence of the longitudinal impedance on the half gap for different wire displacements: once outside of a HOMs the broadband impedance shows the characteristic $1/g$ behavior of a resistive wall longitudinal impedance. Nevertheless, the asymptotic value is determined by the parasitic resistances due to the contacts between the device parts. The contact resistance Z_c contribution is supposed to be constant and it is removed fitting the measurement data with a fitting function $f(g) = \Delta Z_{long}/g + Z_c$, from which the longitudinal impedance ΔZ_{long} is obtained.

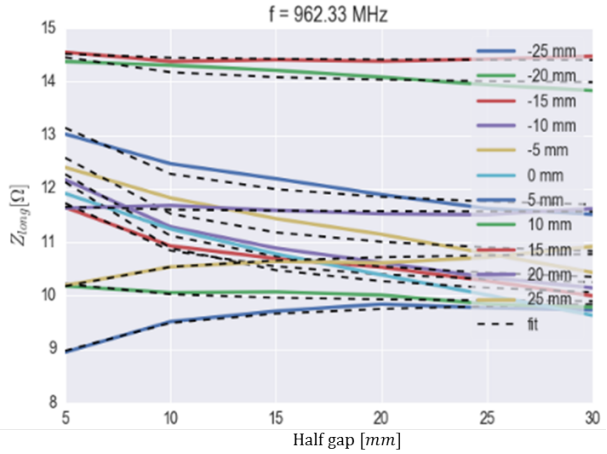

Figure 9: Longitudinal impedance versus gap and wire displacement at 962 MHz together with $1/g$ line fits: the coefficient of the fit determines the impedance.

The result of the fitting procedure is shown in Fig. 10. Few observations can be made:

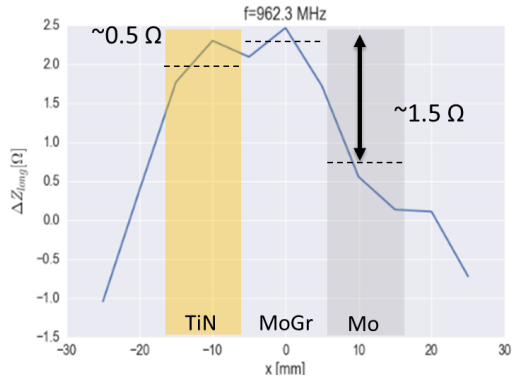

Figure 10: Longitudinal impedance versus horizontal position: a clear reduction is observed for the impedance measured on the Mo and TiN stripe. The largest reduction corresponds to the Mo stripe.

1. For very large displacements the impedance coefficient ΔZ_{long} is found to be negative, or, in other words, the impedance increases versus gap. These positions correspond to the far end of the displacement scan, when the wire is placed on the Glidcop support: enlarging the gap the stainless steel frame is showing more and more, dominating the impedance otherwise negligible.

2. The impedance simulated with IW2D, as shown in Fig. 11, is smaller than measured: this is probably due to the constant additional resistive wall due to the tapered sections made of MoGr. Nevertheless the relative difference is found in very good agreement with measurements.

These two observations will be addressed in more detail in the future with the help of dedicated CST simulations.

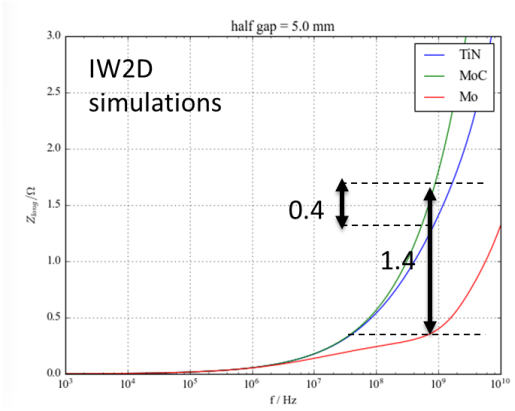

Figure 11: Longitudinal impedance versus horizontal position: IW2D simulations.

Resistivity measurements

In order to correctly model the collimator resistive wall contribution, it is important to evaluate the resistivity of the absorber material. This can be done at DC with standard 4 wires techniques [19], or at RF frequency using a loop antenna [20]. The latter is based on the measurement of the magnetic field induced by the presence of a good conductor in front of a loop antenna as shown in Fig. 12. Comparison of the measured input impedance to the value expected with IW2D simulations allows to deduce the resistivity at each measured frequency. The method has been used to estimate the MoGr resistivity versus frequency as shown in Fig. 13.

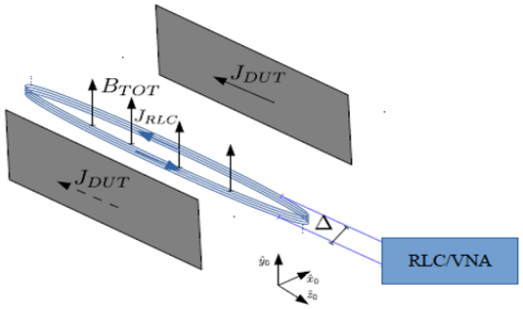

Figure 12: Setup for low frequency resistivity measurements.

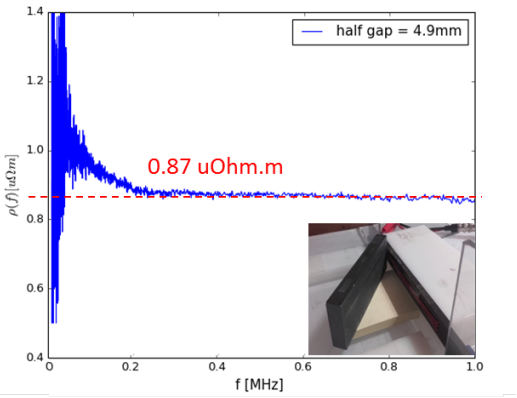

Figure 13: MoGr resistivity versus frequency measured with a loop. The average measurement is close to expected resistivity of 1 uΩm.

The method allows to measure the resistivity of thin films/coatings as well. The application to Mo coating on MoGr is presently under study [21].

Beam based impedance measurements

The quality of an impedance model is subject to the final crosscheck with beam based impedance measurements. One of the standard techniques to measure the transverse impedance of a collimator is the observation of the tune shift induced by the movement of the collimator gap (the impedance is strongly defocussing for small gaps inducing a negative tune shift). CERN collimators have been extensively measured by means of this technique already in the past [22,23], but only recently the method has been improved in a way to boost its resolution down to the 10^{-5} tune shift resolution [8, 24], opening the road for the measurement of the impedance of a single collimator.

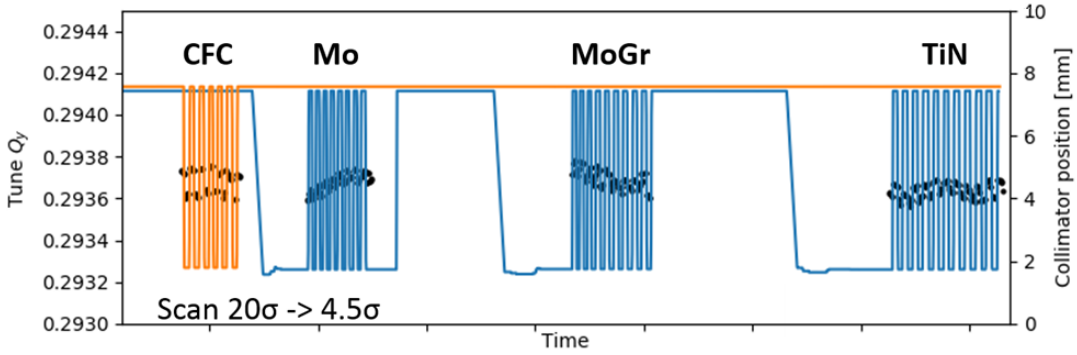

Figure 14: Vertical tune shift measurement versus gap opening for the TCSPM (blue curve) and TCSG.D4R7 (orange curve): the width of the band of dots during the scan is correlated to the collimator transverse reactive impedance.

One of the most interesting applications of the method was the measurement of the impedance of each of the single stripes of the TCSPM collimator. The test is of vital importance as one of the key ingredients for the HL-LHC project is the upgrade of the present collimation system to the new low-impedance collimators featuring (at least for the IR7 collimators) Mo coated MoGr jaws. Figure 14 shows the measured tune while moving the gap of the TCSPM and the adjacent TCSG.D4R7 whose jaw is made of CFC: already by visual inspection it is clear that the Mo stripe presents the least tune shift, i.e. the smallest impedance among the 4 tested materials. Plotting the tune shift versus gap for each of the stripes as shown in Fig. 15, the agreement with the simple 2D model can be appreciated, in particular for the CFC, MoGr and TiN materials. A discrepancy is found for the Mo stripe which is apparently contradicting the longitudinal wire measurements. One of the possible causes is related to the Mo coating surface roughness [25]: the roughness, in first approximation, would mainly affect the inductive impedance, i.e. the tune shift measurements, with negligible impact on the real part of the transverse (and longitudinal) real part of the impedance. This aspect is still presently under investigation.

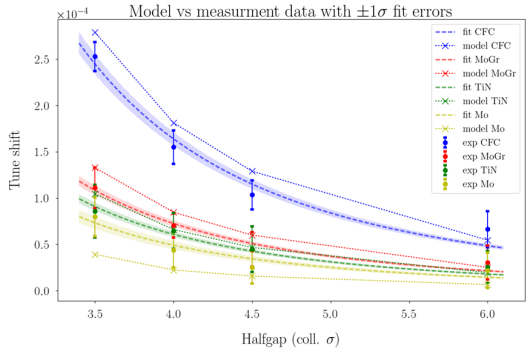

Figure 15: TCSPM and TCSG.D4R7 tune shift versus gap opening. The Mo stripes clearly shows the maximum impedance reduction.

3D COLLIMATOR IMPEDANCE MODELING

Even though it has been proven to be a good approximation, the 2D modeling of a collimator has of course many limitations. When coming to the details of the HOMs modeling, for example, only a complete 3D description of the device allows to obtain precise estimation of the device resonance parameters (frequency, shunt impedance and Q factor). This is the case of the TCTP collimator [26], subject of recent intense studies both with GdfidL and CST: the removal of lateral RF fingers to allow for the space needed by the embedded BPMs, introduced a large cavity volume producing a large number of HOMs. Of these, only part could be suppressed using ferrite tiles as in Fig. 16 and a campaign of simulations and device bench impedance measurements was launched in order to characterize the HOMs and ensure their negligible impact on machine stability.

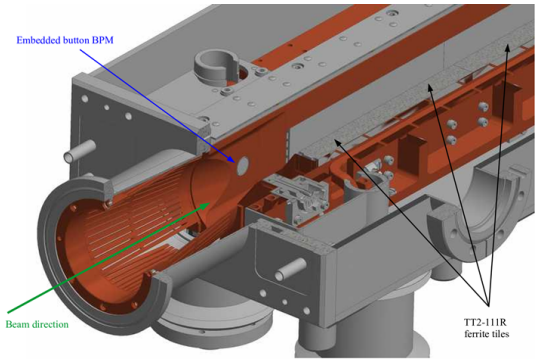

Figure 16: 3D model of the TCTP collimator: ferrite tiles are placed in order to damp the HOMs present in the structure.

Figure 17 shows the effect of the ferrite tiles on the longitudinal impedance: a clear damping effect above 500 MHz can be appreciated. On the other hand, few transverse modes at 82 MHz and 167 MHz are present as shown in Fig. 18.

Bench impedance measurements were performed on the TCTP in order to crosscheck these observations. Indeed, using a probe terminated with a loop, the low frequency

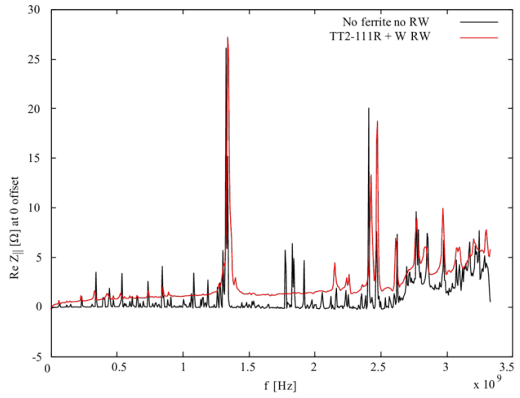

Figure 17: Longitudinal impedance for the new collimator as computed by GdfidL, with (red curve) and without (black curve) TT2-111R ferrite and tungsten resistive wall (W). No offset is applied.

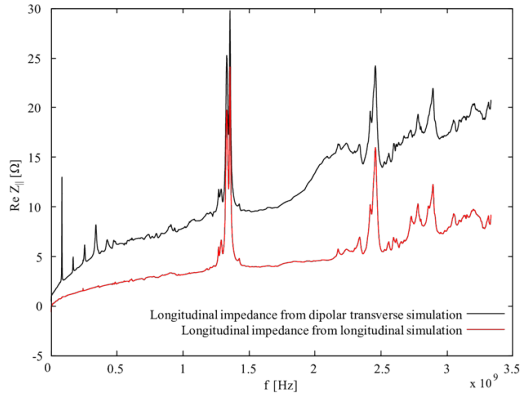

Figure 18: Longitudinal impedances computed for a beam with zero transverse beam offset (red curve) and with a transverse beam offset as done in transverse dipolar impedance simulations (black curve). The computed low frequency HOMs correspond to transverse modes.

HOMs could be detected as shown in Fig. 19 and were found in close agreement with the expected frequency and Q factor.

The shunt impedance was measured with the stretched wire method [27]. The setup was substantially different from the one shown in Fig. 7 as the equivalent coaxial line made by the stretched wire and the device was matched to the characteristic impedance of the device itself. This is done to have finer frequency resolution to localize the HOMs. Unfortunately, the characteristic impedance of a collimator is well defined only for a fixed gap value introducing a mismatch pattern in the measured S21 parameter. This issue can be overcome fitting the baseline mismatch pattern around the HOMs and extracting the information about the shunt impedance. A remarkably good agreement, within a factor of 2, is obtained comparing the measured shunt impedance of the 87 MHz transverse HOMs against GdfidL and CST simulations, as shown in Fig. 20. The discrepancy may depend on several collimator design constraints, namely the gap between the plate where ferrite blocks are installed, the

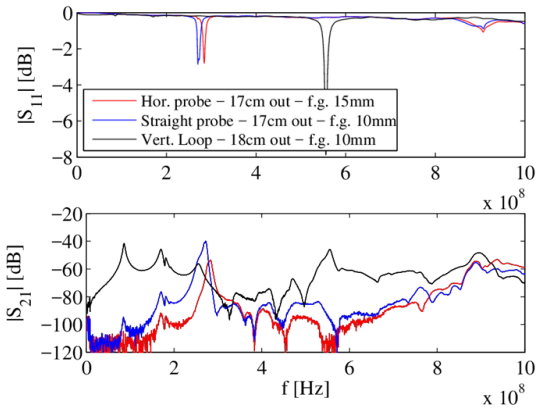

Figure 19: S11 (top) and S21 (bottom) measured with a straight and horizontal probe and with a loop: the low frequency resonant modes exhibit higher coupling through the magnetic field. The first length in the legend refers to the portion of probe outside the device, the second ("f.g.") to the full gap of the collimator.

gap between collimator jaws and external tank and, also, on the mesh and computed wake length [12].

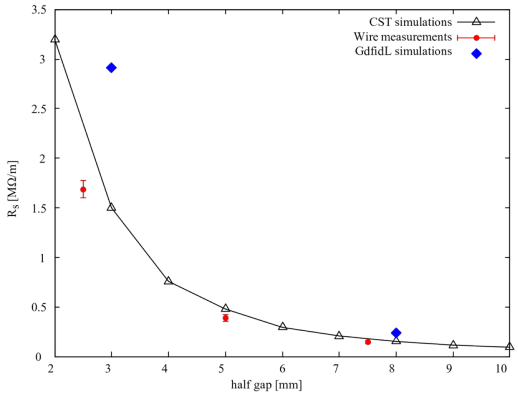

Figure 20: Shunt impedance R s of the 87 MHz mode versus half gap as measured with wire and simulated in CST and GdfidL.

CONCLUSIONS

In this work we have summarized the most common techniques to model the collimator impedance resorting to simple 2D models. In its simplest form a collimator can be assumed to be approximated by two parallel plates of resistive materials. Adding the impedance of the tapers further refines the computed reactive part of the impedance. The modeling is in good agreement both with bench measurement and with beam based tune shift measurements for single collimators in the LHC, where unprecedented accuracy has been recently reached. More complex simulations based on 3D electromagnetic solvers like CST and GdfidL, are needed when, for example, the presence of HOMs in the collimator structure need to be assessed. Bench impedance measurements are in this case of high importance, especially if simplifications

on the mechanical model or on the material properties of dispersive materials (like ferrites) were needed in the simulation phase. Equally important, even though not treated here, are the simulations of the bench impedance measurements and beam based measurements like synchronous phase shift and threshold in octupole strength which give respectively a measurement of the longitudinal real part for the impedance and its impact on transverse stability.

REFERENCES

[1] S. Redaelli. "Beam Cleaning and Collimation Systems". In *Proceedings, 2014 Joint International Accelerator School: Beam Loss and Accelerator Protection: Newport Beach, CA, USA, November 5-14, 2014*, pages 403–437, 2016.

[2] O. Brüning et al. *"LHC Design Report"*. CERN Yellow Reports: Monographs. CERN, Geneva, 2004.

[3] R. Assmann et al. "The final collimation system for the LHC". In *Particle accelerator. Proceedings, 10th European Conference, EPAC 2006, Edinburgh, UK, June 26-30, 2006*, volume C060626, pages 986–988, 2006.

[4] N. Mounet. *"The LHC Transverse Coupled-Bunch Instability"*. PhD thesis, EPFL University, Lausanne, Mar 2012. Presented 2012.

[5] S. Antipov et al. "Machine impedance and HOM power update". 7^{th} HL-LHC collaboration meeting, Madrid, Spain, 2017.

[6] G. Apollinari et al. *"High-Luminosity Large Hadron Collider (HL-LHC): Technical Design Report V. 0.1"*. CERN Yellow Reports: Monographs. CERN, Geneva, 2017.

[7] E. Métral et al. "Update of the HL-LHC operational scenarios for proton operation". Technical Report CERN-ACC-NOTE-2018-0002, CERN, Geneva, Switzerland, Jan 2018.

[8] D. Valuch et al. "Update on single-collimator impedance measurements". COLUSM 75, CERN, Geneva, Switzerland, 19-08-2016.

[9] D. Amorim et al. "Tune shifts: measurements and predictions". COLUSM 91, CERN, Geneva, Switzerland, 11-08-2017.

[10] G. Stupakov. "Low frequency impedance of tapered transitions with arbitrary cross sections". *Phys. Rev. ST Accel. Beams*, 10:094401, Sep 2007.

[11] O. Frasciello et al. "Geometric beam coupling impedance of LHC secondary collimators". *Nuclear Instruments and Methods in Physics Research Section A: Accelerators, Spectrometers, Detectors and Associated Equipment*, 810:68 – 73, 2016.

[12] O. Frasciello. *Wake fields and impedance calculations of LHC collimators' real structures*. PhD thesis, Università degli Studi di Roma "La Sapienza", Feb 2016. Presented 2016.

[13] W. Bruns. `http://www.gdfidl.de`.

[14] K. Yokoya. "Impedance of slowly tapered structures". Technical Report CERN-SL-90-88-AP, CERN, Geneva, Jul 1990.

[15] A. W. Chao and M. Tigner. *"Handbook of Accelerator Physics and Engineering"*. World Scientific, Singapore, 1999.

[16] N. Mounet and E. Métral. "Electromagnetic fields and beam coupling impedances in a multilayer flat chamber". Technical Report CERN-ATS-Note-2010-056 TECH., CERN, Geneva, Switzerland, 2010.

[17] CST Studio Suite®. `http://www.cst.com`.

[18] T. Kroyer, F. Caspers, and E. Gaxiola. "Longitudinal and transverse wire measurements for the evaluation of impedance reduction measures on the MKE extraction kickers". Technical Report AB-Note-2007-028, CERN, Geneva, Switzerland, Jul 2007.

[19] E. Bonanno et al. "Update on conductivity measurements of TDI blocks". Impedance meeting, CERN, Geneva, Switzerland, 25-04-2016.

[20] N. Biancacci et al. "LF impedance measurements on TDI blocks". Impedance meeting, CERN, Geneva, Switzerland, 02-03-2015.

[21] G. Mazzacano et al. "Resistivity measurements on Molybdenum coated CFC and MoGr blocks". Impedance meeting, CERN, Geneva, Switzerland, 08-12-2017.

[22] N. Mounet et al. "Collimator Impedance Measurements in the LHC". Proc. IPAC'13, Shanghai, China, May 2013.

[23] L. Carver et al. "MD 755: Instability threshold and tune shift study with reduced retraction between primary and secondary collimators in IR7". Jan 2016. Rep. CERN-ACC-NOTE-2016-0005.

[24] N. Biancacci et al. "Outcome of TCSG single collimator impedance and instability measurements". LHC Collimation Working Group n.207, CERN, Geneva, Switzerland, 22-08-2016.

[25] J. Guardia Valenzuela et al. "SEM observation of coatings for TCSPM blocks". Impedance meeting, CERN, Geneva, Switzerland, 06-10-2017.

[26] N. Biancacci et al. "Impedance simulations and measurements on the LHC collimators with embedded beam position monitors". *Phys. Rev. Accel. Beams*, 20:011003, Jan 2017.

[27] V. G. Vaccaro. "Coupling impedance measurements: An Improved wire method". Technical Report INFN-TC-94-23, INFN, Naples, Italy, Nov 1994.